Erschienen in: eLife ; 5 (2016). - e18857
http://dx.doi.org/10.7554/eLife.18857

eLIFE elifesciences.org

RESEARCH ARTICLE

Bacterial flagellar capping proteins adopt diverse oligomeric states

Sandra Postel[1], Daniel Deredge[2], Daniel A Bonsor[1], Xiong Yu[3], Kay Diederichs[4], Saskia Helmsing[5], Aviv Vromen[6], Assaf Friedler[6], Michael Hust[5], Edward H Egelman[3], Dorothy Beckett[7], Patrick L Wintrode[2], Eric J Sundberg[1,8,9]*

[1]Institute of Human Virology, University of Maryland School of Medicine, Baltimore, United States; [2]Department of Pharmaceutical Sciences, University of Maryland School of Pharmacy, Baltimore, United States; [3]Department of Biochemistry and Molecular Genetics, University of Virginia, Charlottesville, United States; [4]Department of Biology, University of Konstanz, Konstanz, Germany; [5]Department of Biotechnology, Institute of Biochemistry, Biotechnology and Bioinformatics, Technische Universität Braunschweig, Braunschweig, Germany; [6]Institute of Chemistry, The Hebrew University of Jerusalem, Jerusalem, Israel; [7]Department of Chemistry and Biochemistry, University of Maryland College Park, Baltimore, United States; [8]Department of Medicine, University of Maryland School of Medicine, Baltimore, United States; [9]Department of Microbiology and Immunology, University of Maryland School of Medicine, Baltimore, United States

Abstract Flagella are crucial for bacterial motility and pathogenesis. The flagellar capping protein (FliD) regulates filament assembly by chaperoning and sorting flagellin (FliC) proteins after they traverse the hollow filament and exit the growing flagellum tip. In the absence of FliD, flagella are not formed, resulting in impaired motility and infectivity. Here, we report the 2.2 Å resolution X-ray crystal structure of FliD from *Pseudomonas aeruginosa*, the first high-resolution structure of any FliD protein from any bacterium. Using this evidence in combination with a multitude of biophysical and functional analyses, we find that *Pseudomonas* FliD exhibits unexpected structural similarity to other flagellar proteins at the domain level, adopts a unique hexameric oligomeric state, and depends on flexible determinants for oligomerization. Considering that the flagellin filaments on which FliD oligomers are affixed vary in protofilament number between bacteria, our results suggest that FliD oligomer stoichiometries vary across bacteria to complement their filament assemblies.
DOI: 10.7554/eLife.18857.001

***For correspondence:** esundberg@ihv.umaryland.edu

Competing interest: See page 17

Funding: See page 17

Received: 15 June 2016
Accepted: 23 September 2016
Published: 24 September 2016

Reviewing editor: Richard M Berry, University of Oxford, United Kingdom

Introduction

Pathogenic bacteria cause a multitude of deadly human diseases. Many of these microbes possess flagella, molecular machines responsible for cell motility, adherence to host cells, and pathogenicity (***Duan et al., 2013***; ***Haiko and Westerlund-Wikstrom, 2013***). Flagella are helix-shaped hollow attachments formed predominantly by thousands of copies of the protein flagellin (also called FliC), anchored in the bacterial membrane by a hook (or joint) that is attached to the basal body and that is composed of rotary motor proteins (***Arora et al., 1998***). A proton motive force typically drives the propeller motion of flagella (***Berg, 2003***), resulting in swimming motility. A FliD (also called HAP2) oligomer forms the cap protein complex that is located at the tip of the flagellar filament (***Yonekura et al., 2000***). This complex controls the distal growth of the filament by regulating the

eLife digest Many bacteria, including several that cause diseases in people, have long whip-like appendages called flagella that extend well beyond their cell walls. Flagella can rotate and propel the bacteria through liquids, such as water or blood, and they are constructed primarily from thousands of copies of a single protein called flagellin. When flagella are built, the flagellin proteins are placed in their proper positions by another protein called FliD, several copies of which form a cap on the end of flagella. Without FliD, bacteria cannot properly assemble flagella and, thus, can no longer swim; this also hinders their ability to cause disease.

Determining the three-dimensional structure of a protein, down to the level of its individual atoms, can provide unique insights into how the protein operates. However, no one had resolved the structure of a FliD protein from any bacterium to this level of detail before.

Now, Postel et al. report the high-resolution structure of a large fragment of FliD from the bacterium *Pseudomonas aeruginosa*. The structure reveals that parts of this FliD protein are shaped like parts of other proteins from which flagella are constructed, including the flagellin protein that FliD places into position. Some parts of the FliD protein are also very flexible and these parts of the protein are responsible for holding numerous FliD proteins together as a cap. Finally, Postel et al. saw that six copies of FliD bind to one another to form a protein complex on the end of flagella. This last finding was particularly unexpected since it was thought that all FliD proteins formed five-membered cap complexes, an assumption that was based largely on studies of FliD from another bacterium called *Salmonella*.

The current structure covers about half of the FliD protein, and so the next challenge is to determine the structure of the full-length protein. An improved understanding of the structure of FliD may, in future, help researchers to design drugs that stop bacteria from building flagella and, therefore, from swimming and causing disease.

DOI: 10.7554/eLife.18857.002

assembly of FliC molecules, which are transported through the hollow filament from the cytoplasm to the tip of the flagellum.

The dynamic movement of FliD in this assembly was modeled based on low (~26 Å)-resolution cryo-electron microscopic (EM) structures of the *Salmonella* serovar Typhimurium flagellum-cap complex (**Maki-Yonekura et al., 2003**; **Yonekura et al., 2000**, **2003**), which adopts the shape of a five-legged stool with flexible leg domains that regulate the assembly of new FliC molecules onto the tip of the growing flagellum (**Maki-Yonekura et al., 2003**). It has been suggested that the plate of the stool is formed by core regions of the FliD molecule, and that disordered/flexible regions form the five leg structures (**Vonderviszt et al., 1998**) that are known to interact with the FliC filament. FliD exhibits low sequence similarity to the flagellar hook proteins and to FliC. Nevertheless, it shares the disordered terminal regions of these flagellar proteins, a common structural characteristic that is thought to control the polymerization of flagellar proteins and to play an important role in interaction with the FliC filament (**Vonderviszt et al., 1998**). These regions are the most conserved in FliD sequences across bacteria. Flagellum-mediated motility is crucial for the virulence and pathogenicity of numerous bacteria, including *Campylobacter jejuni* (**Black et al., 1988**), *Salmonella* (**Allen-Vercoe and Woodward, 1999**; **Marchetti et al., 2004**), *Escherichia coli* (**La Ragione et al., 2000**), *Vibrio cholera* (**Krukonis and DiRita, 2003**), and *Pseudomonas aeruginosa* (**Arora et al., 2005**), as well as the major causative agent of gastric cancer *Helicobacter pylori* (**Kim et al., 1999**). To date, however, no high-resolution structure of any FliD protein exists. To better define the roles of FliD in bacterial motility and pathogenesis, we determined the first X-ray crystal structure of FliD at 2.2 Å resolution, and assessed the structural contributions of its flexible regions using a multitude of complementary biophysical and functional analyses.

Results

Crystal structure of the FliD protein from *P. aeruginosa* PAO1

To facilitate crystallization of FliD from the *P. aeruginosa* PAO1 strain, we deleted the predicted coiled-coil domains on both the N- and C-termini of full length FliD, which has 474 residues ($FliD_{1–474}$), to generate the truncated $FliD_{78-405}$ (***Figure 1a***, ***Figure 1—source data 1***). We expressed $FliD_{78–405}$ in *E. coli* with an N-terminal His_6-tag and purified it to homogeneity by Ni^{2+}-NTA, size exclusion and anion exchange chromatography. We improved initially weakly diffracting crystals of $FliD_{78–405}$ by random matrix microseed screening (***Bergfors, 2003***), yielding crystals that diffracted to 2.2 Å resolution. In the absence of any homologous protein that could be used as a model for molecular replacement, we crystallized a seleno-methionine derivative of $FliD_{78–405}$ that included four leucine-to-methionine mutations ($FliD_{78–405}/L_4–M_4$). This crystal provided phase information sufficient to build an initial model, which we used subsequently for molecular replacement with the native $FliD_{78–405}$ dataset (***Figure 1—source data 1***). We modeled residues 80–273 into clear electron density, including all side chains, but observed density of increasingly poor quality in the C-terminus beyond residue 273 (***Figure 1—figure supplement 2a***). Thus, we were able to model with

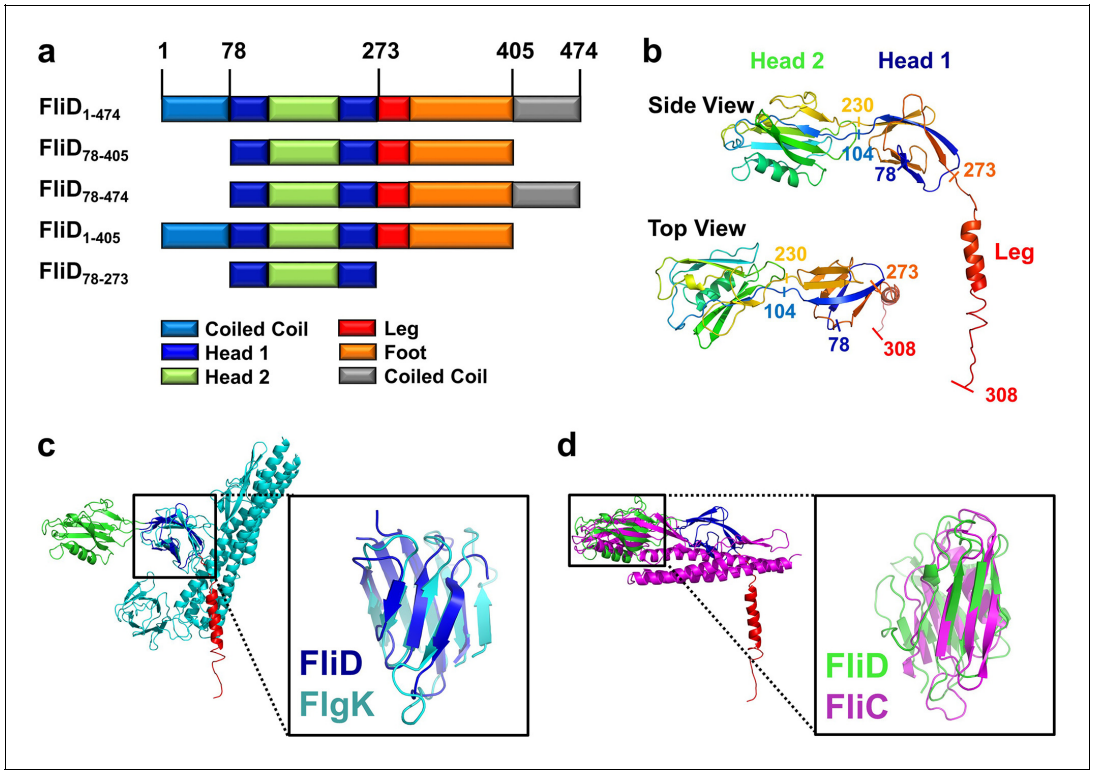

Figure 1. Crystal structure of *Pseudomonas* FliD reveals structural similarity to other flagellar proteins. (**a**) Schematic representation of the FliD proteins used in these studies. Protein domain/region boundaries are labeled and are drawn approximately to scale. (**b**) Crystal structure of the *Pseudomonas* $FliD_{78–405}$ monomer subunit with spectrum coloring from the N-terminus (blue) to the C-terminus (red). Head domain 1, head domain 2 and the leg region are indicated. (**c**) Superposition of the $FliD_{78–405}$ crystal structure (domain coloring as in panel (a)) and *Burkholderia* FlgK/HAP1/hook filament capping protein (cyan). (**d**) Superposition of the $FliD_{78–405}$ crystal structure (domain coloring as in panel (a)) and *Pseudomonas* flagellin/FliC (magenta).
DOI: 10.7554/eLife.18857.003
The following source data and figure supplements are available for figure 1:

Source data 1. Crystallographic data collection, phasing and refinement statistics.
DOI: 10.7554/eLife.18857.004
Figure supplement 1. Protein sequence of $FliD_{1–474}$.
DOI: 10.7554/eLife.18857.005
Figure supplement 2. Electron density and protein degradation of FliD crystals.
DOI: 10.7554/eLife.18857.006

confidence only a single α helix in this region, corresponding to residues 274–308, with incomplete side chain structures. To determine whether the remaining region of the protein actually existed in the crystals and not just in the protein preparation used for crystallization, we analyzed crystals using liquid chromatography-mass spectrometry (LC-MS) and SDS-PAGE. Both analyses indicated that the crystals consisted of an approximate 50:50 mixture of the $FliD_{78–405}$ protein used for crystallization and a further proteolyzed version with a molecular weight of about 27 kDa. The N-terminal His_6-tag is still detectable by Western blot (***Figure 1—figure supplement 2b***). Thus, the proteolyzed form corresponds approximately to residues 78–319 of FliD. The 86 residues absent from the C-terminus in a population of FliD proteins are clearly not required for crystal packing, suggesting that they are highly flexible even in a crystalline environment.

FliD is structurally similar on the domain level to FliC and FlgK

Our crystal structure of $FliD_{78–405}$ reveals that it consists of two discreet regions with distinct conformational properties, corresponding to a stable head region and a flexible and/or disordered leg region (***Figure 1b***). The head region is itself comprised of two separate, but entwined, protein domains. Residues 80–101 form two β strands that belong to the first domain (Head 1), the second domain (Head 2) is formed in its entirety by the contiguous residues 104–230, and residues 231–273 then complete the first domain. The second domain is, thus, a loop insertion of the first domain. We searched for structural homologs of these domains in the Protein Data Bank and found that the first domain of the head region (Head 1) exhibits high structural similarity (RMSD=2.5 Å), despite low sequence identity (14%), to the FlgK/HAP1/hook filament capping protein of *Burkholderia pseudomallei* (PDB code 4UT1; ***Figure 1c***). Likewise, the second head region domain (Head 2) exhibits high structural similarity (RMSD=2.7 Å), despite low sequence identity (17%), to the FliC/flagellin protein of *P. aeruginosa* (PDB code 4NX9; ***Figure 1d***). In contrast to the head region, the leg region of FliD is highly flexible, as indicated by the paucity of electron density corresponding to residues 274–405 (***Figure 1—figure supplement 2a***). Despite this, we were able to model the initial α helical structural element, corresponding to residues 274–308, of this region. This helix extends from the axis of the head region at a nearly perpendicular angle, resulting in an L-shaped monomer subunit structure (***Figure 1b***).

FliD from *P. aeruginosa* PAO1 forms a hexamer

In the crystal, $FliD_{78–405}$ monomer subunits are arranged in hexamers, resulting in a shape akin to a six-pointed star when viewed from the top of the FliD oligomer (***Figure 2a***), which corresponds to the distal end of the growing flagellum. This star shape has a minimum inner diameter of 48 Å and a maximal outer diameter of 136 Å. When viewed from the side (***Figure 2b***), the FliD hexamer appears as a six-legged stool, the legs of which extend 55 Å below the bottom of the head region. Additional crystallographic symmetry results in the stacking of hexamers in alternating head-to-head and leg-to-leg orientations (***Figure 2c***). The leg-to-leg stacking forms dodecamers, resulting from the helix–helix interaction of the residues 274–302 of stacked molecules and the interaction of residues 303–308 of one $FliD_{78–405}$ molecule with Head 1 domain of a stacked molecule, burying a surface area of 1362 $Å^2$. The formation of dodecamers may be unique to the $FliD_{78–405}$ fragment, as this strand could potentially be replaced by additional N-terminal residues in the full-length $FliD_{1–474}$ protein. All of the morphologies observed for *Pseudomonas* FliD are highly reminiscent of the pentamer/decamer oligomeric organization of *Salmonella* FliD as determined by low-resolution cryo-EM analysis (***Maki-Yonekura et al., 2003***) (***Figure 2d***). Indeed, despite the difference in the stoichiometries of the *Pseudomonas* and *Salmonella* FliD oligomers, the gross measurements are nearly identical for these two proteins of similar molecular weight. In our crystal structure, *Pseudomonas* FliD measures 136 Å in diameter with a head region that is 30 Å deep and a leg region that is 55 Å long; whereas, in the cryo-EM structure, *Salmonella* FliD measures 145 Å in diameter with a head region that is 30 Å deep and a leg region that is 55 Å long (***Maki-Yonekura et al., 2003***).

The stoichiometry of *Pseudomonas* FliD differs from that of *Salmonella* FliD and our *Pseudomonas* FliD crystals belong to the *P6* space group, which could possibly force a non-physiological oligomeric organization of subunits. Thus, we confirmed that the hexameric assembly of $FliD_{78–405}$ occurs not only in the crystalline environment but also in solution using negative stain EM class averaging

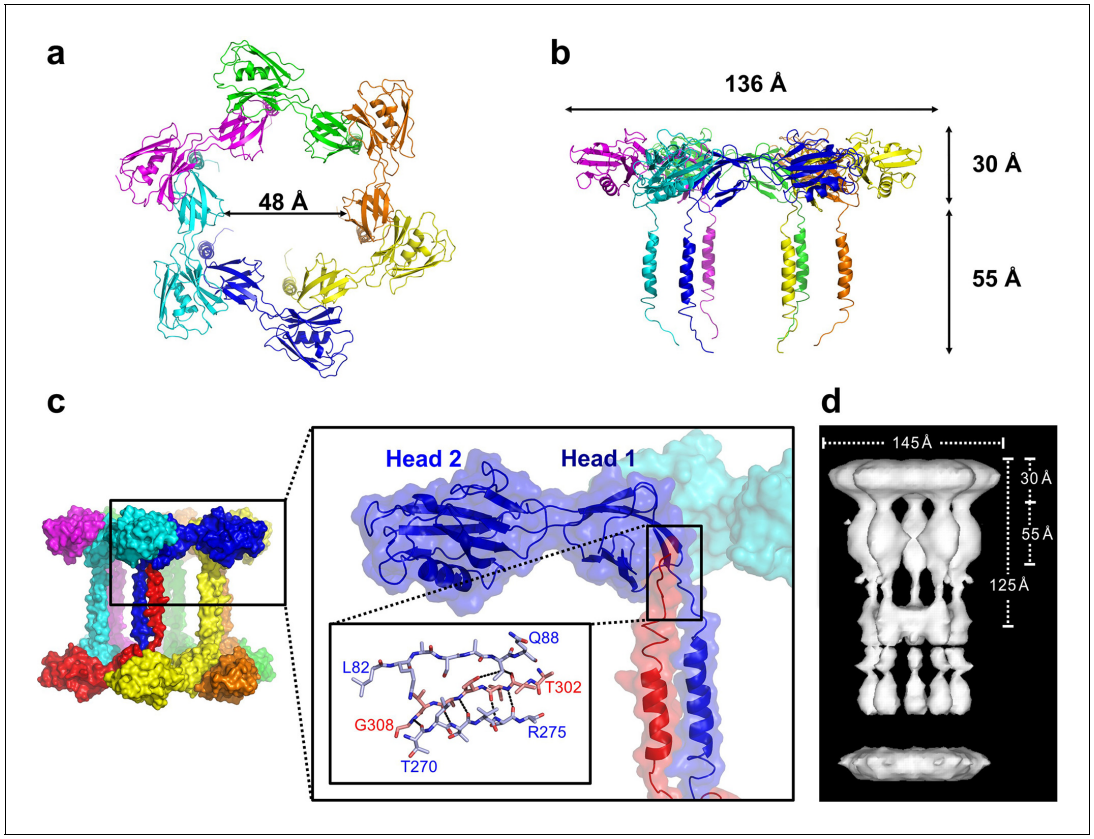

Figure 2. *Pseudomonas* FliD forms hexamers in crystals. (**a**) Top view, cartoon representation of the $FliD_{78–405}$ hexamer. Each monomer subunit is colored distinctly and inner diameter dimension is indicated. (**b**) Side view, cartoon representation of the $FliD_{78–405}$ hexamer. Each monomer subunit is colored distinctly. Outer dimensions are indicated. (**c**) $FliD_{78–405}$ hexamers as arranged in the crystal are stacked head-to-head and leg-to-leg (shown) in an alternating fashion, with residues 303–308 assembling in the Head 1 domain of an opposing molecule (close-up views) leading to a dodecameric crystal packing. (**d**) Cryo-EM structure of *Salmonella* FliD from (***Maki-Yonekura et al., 2003***) for comparison.
DOI: 10.7554/eLife.18857.007

(***Tang et al., 2007***), resulting in an image that clearly exhibits a hexameric assembly (***Figure 3a***). These data are consistent with the oligomerization state that we detected in the crystal structure, in which a view looking down the α-helices of the leg reveals a six-membered ring organization. We also verified that both $FliD_{78–405}$ and full-length $FliD_{1–474}$ form oligomers by both analytical ultracentrifugation (AUC) and crosslinking analyses. We found that the $FliD_{78–405}$ fragment that we crystallized oligomerizes up to a dodecameric state (***Figure 3b,c***), similar to the crystallographic assembly (***Figure 2c***). Additionally, we collected small-angle X-ray scattering (SAXS) data of $FliD_{78–405}$, for which the calculated radial distribution function (***Figure 3d***) is characteristic of an oligomeric assembly forming a hollow sphere (***Svergun and Koch, 2003***). These data produce a molecular envelope that superimposes well with our dodecameric $FliD_{78–405}$ X-ray crystal structure (***Figure 3d***). Full-length $FliD_{1–474}$, by contrast, forms up to hexamers in solution (***Figure 3e,f***), which are likely to represent the physiologically relevant oligomerization state of this protein on the tip of the flagellum. The predominant tetrameric species in solution identified by AUC may be a stable intermediate on the path to hexamer formation (***Figure 3e***).

As the hexameric assembly of full-length *Pseudomonas* $FliD_{1–474}$ proved to be unstable in solution in the absence of the flagellar filament, we sought to stabilize it using our newfound understanding of its structure. We used our crystal structure of $FliD_{78–405}$, as input to Disulfide by Design 2.0 (***Craig and Dombkowski, 2013***), to identify cysteine mutations that would lead to a stable, disulfide-bridged hexameric $FliD_{1–474}$. We found that when two residues within neighboring head domain subunits, I167 and D253, were each mutated to a cysteine residue (***Figure 4a***) a stable, hexameric full-length $FliD_{1–474(I167C/D253C)}$ resulted under non-reducing conditions, as shown by SDS-PAGE

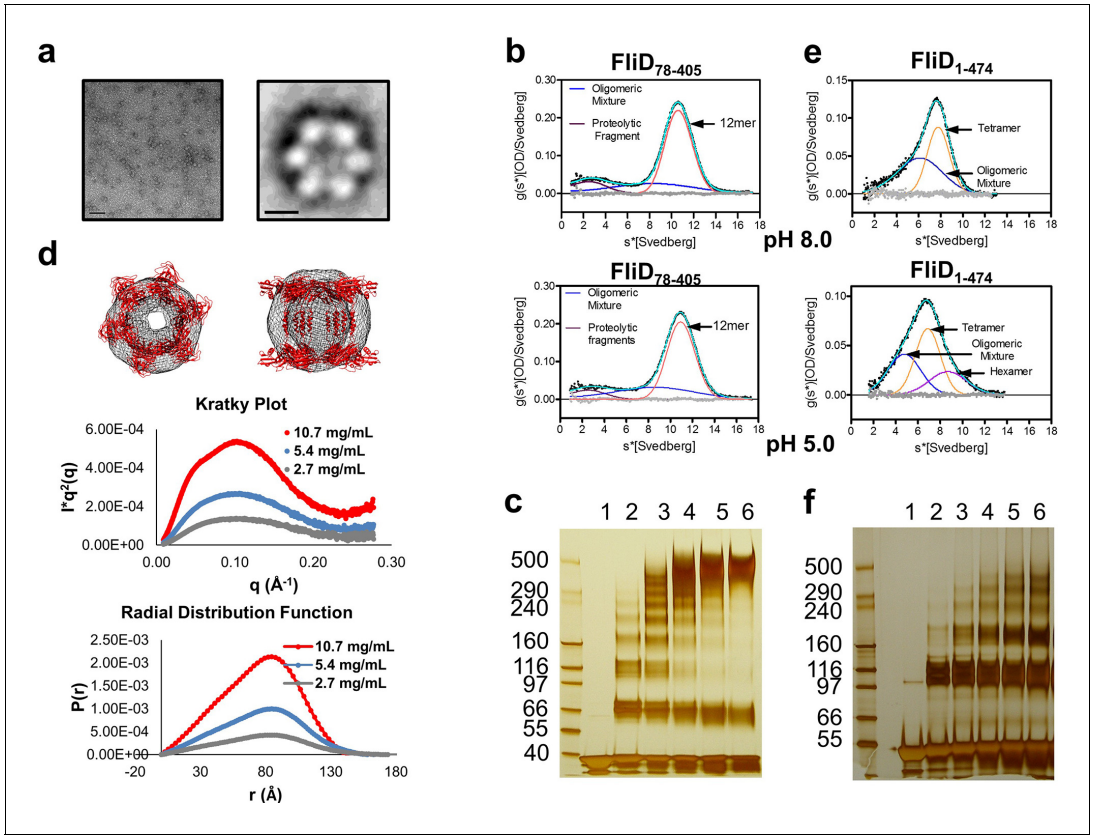

Figure 3. *Pseudomonas* FliD oligomerization. (**a**) Negative stain EM image of $FliD_{78–405}$: left, single particles (scale bar=1000 Å); right, class-averaged particle (scale bar=50 Å). (**b**) AUC analysis of $FliD_{78–405}$ proteins at pH 8.0 (upper panel) and pH 5.0 (lowel panel) indicates that it forms dodecamers in solution. (**c**) Silver-stained SDS-PAGE after chemical crosslinking of $FliD_{78–405}$. (**d**) SAXS analysis of $FliD_{78–405}$. Kratky plot (I^*q^2 *versus* q) and radial distribution function calculated by GNOM, and SAXS envelopes calculated by DAMMIF, with superimposed crystal structures are shown for $FliD_{78–405}$ at 10.7 mg/mL (red, used to calculate envelope), 5.4 mg/mL (blue) and 2.7 mg/mL (grey). (**e**) AUC analysis of full length $FliD_{1–474}$ proteins at pH 8.0 (upper panel) and pH 5.0 (lower panel) indicates a mixture of oligomers, including tetramers and hexamers. (**f**) Silver-stained SDS-PAGE after chemical crosslinking of $FliD_{1–474}$.

DOI: 10.7554/eLife.18857.008

(***Figure 4b***) and SAXS (***Figure 4c***) analyses. We also confirmed that the cysteine bridges resulted in the expected interfaces between head domains by employing mass spectrometry to compare the peptide coverage under reducing and non-reducing conditions (***Figure 4—figure supplement 1a***) and by successfully detecting the correct cysteine bridges (C167–C253) while ruling out non-specific cysteine bridging (C167–C167 and C253–C253) (***Figure 4—figure supplement 1b–e***).

To show that the hexameric form of *Pseudomonas* FliD is functional in vivo, we complemented the *fliD* transposon strain PW2975 (Δ*fliD*) with wildtype $fliD_{1–474}$ and hexamer-stabilized $fliD_{1–474\,(I167C/D253C)}$, resulting in *Pseudomonas* PAO1 strains Δ*fliD*/$fliD_{1–474}$ and Δ*fliD*/$fliD_{1–474(I167C/D253C)}$, respectively. We found that swimming motility that was lost in the Δ*fliD* strain was restored in both Δ*fliD*/$fliD_{1–474}$ and Δ*fliD*/$fliD_{1–474(I167C/D253C)}$ complementation strains, similar to our observations in the wildtype *Pseudomonas* PAO1 strain (***Figure 4d***). Using antibodies that we generated by phage display to *Pseudomonas* PAO1 FliD, we confirmed the expression of full-length FliD proteins by Western blot analysis from preparations of flagella isolated from live bacteria from both Δ*fliD*/$fliD_{1–474}$ and Δ*fliD*/$fliD_{1–474(I167C/D253C)}$ complementation strains (***Figure 4e***). In flagella preparations from the Δ*fliD*/$fliD_{1–474(I167C/D253C)}$ complementation strain, the $FliD_{1–474(I167C/D253C)}$ protein produced by *Pseudomonas* maintains its hexameric oligomeric state (***Figure 4e***). In contrast, subsequent to flagella isolation from live bacteria, $FliD_{1–474}$ does not maintain a stable hexameric complex in either the wildtype *Pseudomonas* PAO1 strain or in the Δ*fliD*/$fliD_{1–474}$ complementation strain (***Figure 4e***). The Δ*fliD* transposon strain does not form flagella, as indicated by the lack of FliC in the analyzed

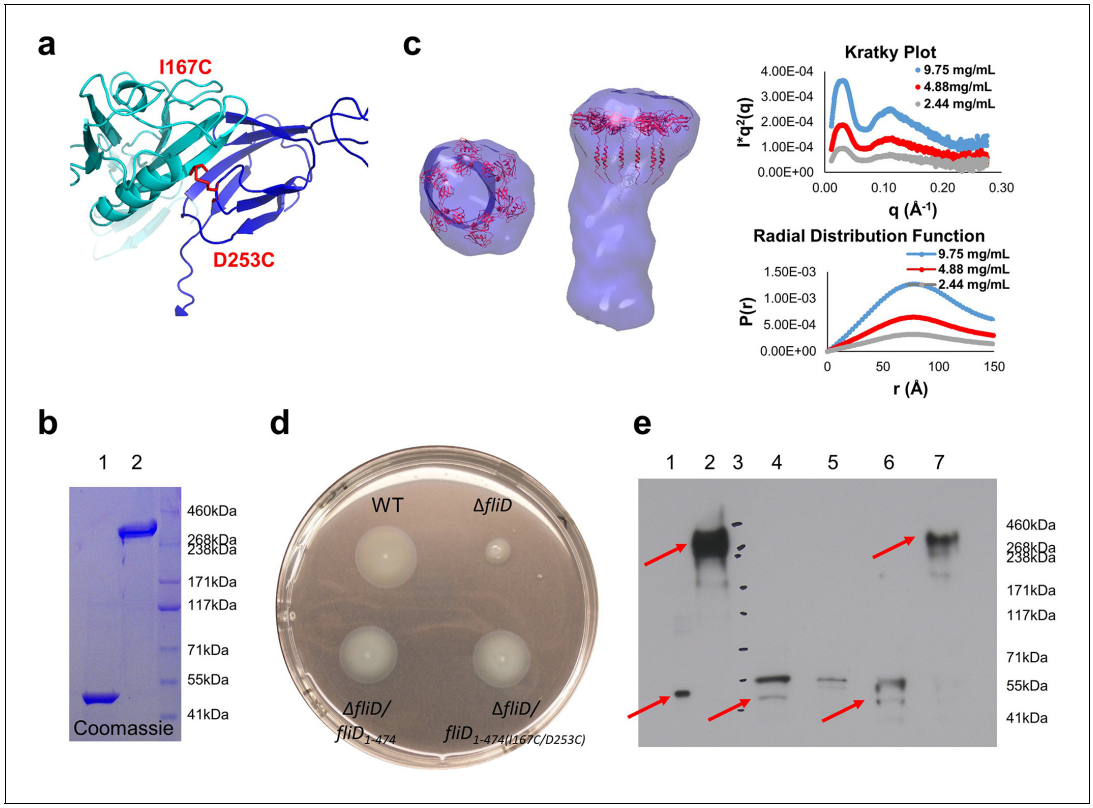

Figure 4. Stable hexameric DM1-FliD$_{1–474}$ complements *P. aeruginosa* PAO1 dFliD transposon strain. (**a**) Location of residues I167 and D253, which were predicted by the web server Disulfide by Design 2.0 (***Craig and Dombkowski, 2013***) to form stable disulfide bridges after mutation to cysteines. (**b**) FliD$_{1–474(I167C/D253C)}$ analyzed under reducing (lane 1) and non-reducing (lane 2) conditions by SDS-PAGE. (**c**) SAXS analysis of FliD$_{1–474(I167C/D253C)}$. Kratky plot (I^*q^2 *versus* q) and radial distribution function calculated by GNOM for 9.75 mg/mL (blue, used to calculate envelope), 4.88 mg/mL (red) and 2.44 mg/mL (grey). SAXS envelope calculated by DAMMIF with superimposed FliD$_{78–405}$ crystal structure. (**d**) Swimming motility assay of wildtype PAO1 (WT), FliD transposon strain PW2975 (Δ*fliD*), Δ*fliD* complemented with FliD$_{1–474}$ (Δ*fliD/fliD*$_{1–474}$) or FliD$_{1–474(I167C/D253C)}$ (Δ*fliD/fliD*$_{1–474(I167C/D253C)}$), respectively. (**e**) Western blot using anti-FliD scFv-Fc SH1579-B7 showing purified protein FliD$_{1–474(I167C/D253C)}$ under reducing (lane 1) and under non-reducing (lane 2) conditions. The presence of FliD in flagella preparations from wildtype PAO1 (lane 4), Δ*fliD* (lane 5), Δ*fliD/fliD*$_{1–474}$(lane 6) and Δ*fliD/fliD*$_{1–474(I167C/D253C)}$ (lane 7) was analyzed under non-reducing conditions. The molecular weight standard is shown in lane 3 and the corresponding molecular weights are indicated on the right side of the blot. The 50 kDa and the 300 kDa bands representing FliD$_{1–474}$ or hexameric FliD$_{1–474(I167C/D253C)}$, respectively, are indicated by red arrows.

DOI: 10.7554/eLife.18857.009

The following figure supplements are available for figure 4:

Figure supplement 1. Analysis of FliD$_{1–474(I167C/D253C)}$ peptides following pepsin digestion under reducing and non-reducing conditions.

DOI: 10.7554/eLife.18857.010

Figure supplement 2. Western blot analysis of PAO1 strain flagella preparations.

DOI: 10.7554/eLife.18857.011

Figure supplement 3. Swimming motility assay.

DOI: 10.7554/eLife.18857.012

flagella preparations (lane 5 on the stained Western blot membrane, ***Figure 4—figure supplement 2***). In comparison, the wildtype and all complementation strains form flagella as indicated by the presence of flagellin/FliC in the purified flagella samples (***Figure 4—figure supplement 2***). Together, these data indicate that FliD that is covalently locked in its hexameric assembly can form functional flagella that allow *Pseudomonas* bacteria to swim like *Pseudomonas* with wildtype FliD. Thus, the hexamer oligomeric state of *Pseudomonas* FliD is functional in vivo.

We also tested whether *Salmonella* FliD, which is known to form pentamers when capping the flagellar filament, could function as a capping protein for *Pseudomonas* flagella. In contrast to the in vivo functional hexameric forms of *P. aeruginosa* FliD$_{–474}$, complementation of the PAO1 PW2975 transposon strain with *fliD* from *Salmonella typhimurium* (Δ*fliD/fliD*$_{StyFliDe}$) did not restore swimming

motility (***Figure 4—figure supplement 3***). As this clone was codon-optimized for expression in *Escherichia coli*, we also confirmed that a wildtype PAO1 full-length $FliD_{1–474}$ encoded by a similarly codon-optimized gene did restore swimming motility in the ΔfliD strain (Δ*fliD/fliD*$_{PAOfliDe}$; ***Figure 4—figure supplement 3***). Although there exist many possible reasons other than oligomeric state that could explain the inability of *Salmonella* FliD to functionally complement *Pseudomonas*, these data suggest that *Pseudomonas* flagella may prefer FliD proteins that adopt hexameric rather than pentameric states.

Regions outside of the head domains drive FliD oligomerization

Although the $FliD_{78–405}$ crystal structure exhibits intermolecular contacts between the head regions of $FliD_{78–405}$ subunits comprising the hexamer, each of these interfaces is small, with a buried surface area of only 665 Å^2, and contains few intermolecular contacts (***Figure 5a***) relative to typical protein–protein interactions (***Jones and Thornton, 1996***). To determine whether these interactions were sufficient to drive oligomerization of FliD, we expressed and purified the head region only, $FliD_{78–273}$. By AUC (***Figure 5b***), chemical crosslinking (***Figure 5c***) and SAXS analysis (***Figure 5d***), we observed that when FliD lacks the leg region and the N- and C-terminal coiled-coil domains, it is present predominantly in the form of monomers (and dimers to a lesser extent) in solution, but fails to form higher-order oligomers as do the longer versions of FliD that we analyzed. Because different buffer

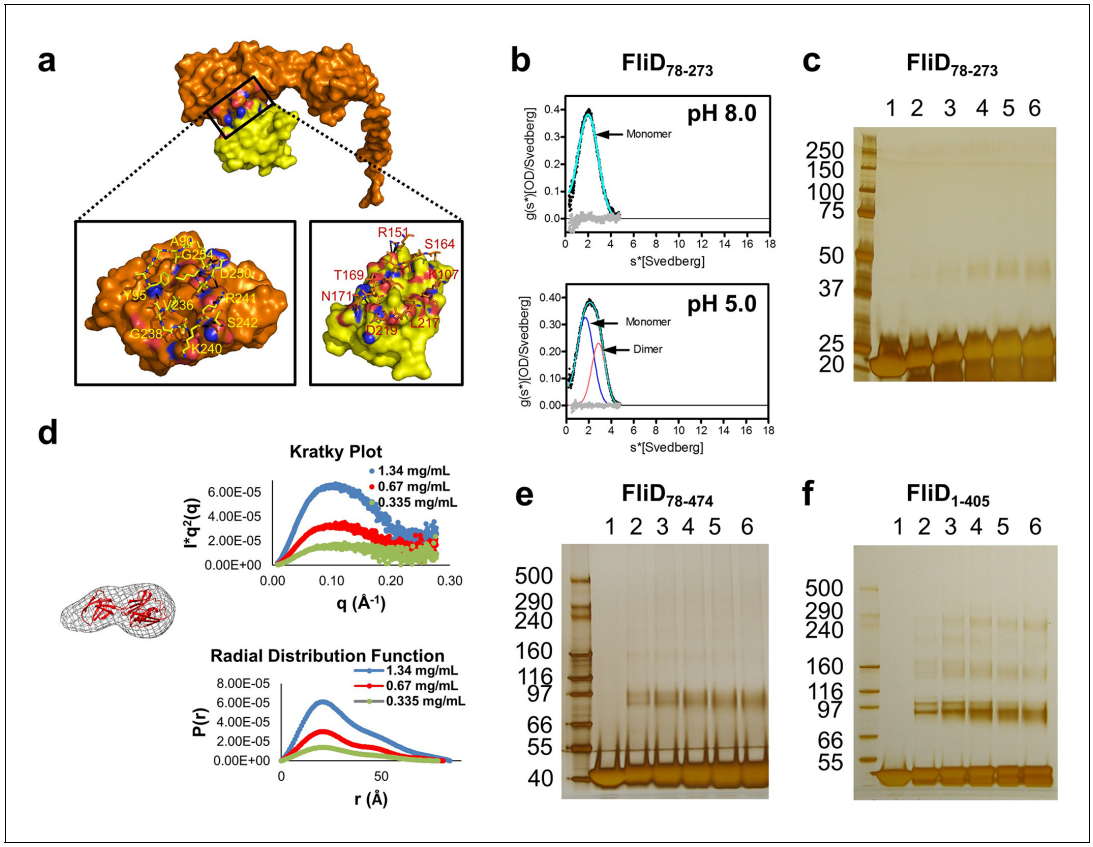

Figure 5. Molecular determinants of *Pseudomonas* FliD oligomerization reside outside of the stable head region. (**a**) Intermolecular interface formed between head region monomer subunits, with an 'open book' rendering of the interface expanded below. Head domain 1 is yellow; domain 2 is orange; interface oxygen and nitrogen atoms are red and blue, respectively. (**b**) AUC analysis of the head region alone, $FliD_{78–273}$, at pH 8.0 (upper panel) and pH 5.0 (lower panel) reveals a monomeric species at pH 8.0 and the additional minor presence of a dimeric species at pH 5.0. (**c**) Silver-stained SDS-PAGE after chemical crosslinking of $FliD_{78–273}$. (**d**) SAXS analysis of $FliD_{78–273}$. Kratky plot (I^*q^2 *versus* q) and radial distribution function calculated by GNOM and SAXS envelopes calculated by DAMMIF with superimposed crystal structures are shown for $FliD_{7–273}$ at 1.34 mg/mL (blue), 0.67 mg/mL (red, used to calculate the envelope) and 0.335 mg/mL (green). (**e**) Silver-stained SDS-PAGE after chemical crosslinking of $FliD_{78–474}$. (**f**) Silver-stained SDS-PAGE after chemical crosslinking of $FliD_{1–405}$.

DOI: 10.7554/eLife.18857.013

conditions, including changes in pH, have been shown to affect the polymerization states of flagellar filaments (***Shibata et al., 2005***) and capping proteins (***Imada et al., 1998***), we performed additional AUC experiments and found that $FliD_{78–273}$ is entirely monomeric at pH 8.0 and becomes approximately one-third dimeric at pH 5.0; we observed no higher-order oligomers of $FliD_{78–273}$ regardless of buffer conditions (***Figure 5b***). We also assessed, by chemical cross-linking, the oligomerization states of FliD variants lacking only the N-terminal coiled-coil domain ($FliD_{78–474}$; ***Figure 5e***) or the C-terminal coiled-coil domain ($FliD_{1–405}$; ***Figure 5f***). We found them to be mainly monomeric with a minority of species appearing to dimerize, although the latter exhibit weak higher-order oligomerization potential. Kratky plots and radial distribution functions calculated from SAXS data of the variants lacking either the N- or C-terminal coiled-coil domain, $FliD_{78–474}$ or $FliD_{1–405}$ respectively, reveal that these proteins adopt extended shapes with flexible regions that are clearly represented in the resulting molecular envelopes (***Figure 6a,b***). These data indicate that the driving force for hexamerization of *Pseudomonas* FliD resides in molecular determinants outside of the head region and, at a minimum, involves residues in the N-terminal and C-terminal coiled-coil domains. $FliD_{78–405}$ is lacking the C-terminal and N-terminal coiled-coil domain but still assembles into dodecamers, as shown in the crystal structure, cross-linking experiments and AUC, which is likely caused by strand replacement in the head region domain 1 and helix–helix (residues 274–308) interaction of stacked molecules (***Figure 2c***).

The N- and C-terminal regions of FliD are highly flexible

A large extent of FliD sequence currently remains inaccessible to high-resolution structural analysis, including *Pseudomonas* FliD residues 1–79 and 309–474. Consequently, we performed hydrogen/deuterium (H/D) exchange-mass spectrometry (HDX-MS) experiments with $FliD_{78–405}$ to define its solvent accessible regions and to evaluate its dynamic behavior. We subjected $FliD_{78–405}$ to H/D exchange for 10 s to 2 hr and observed that the head region (residues 80–273) of $FliD_{78–405}$ adopts a largely stable exchange-protected fold with greater stability observed for domain 2 relative to that

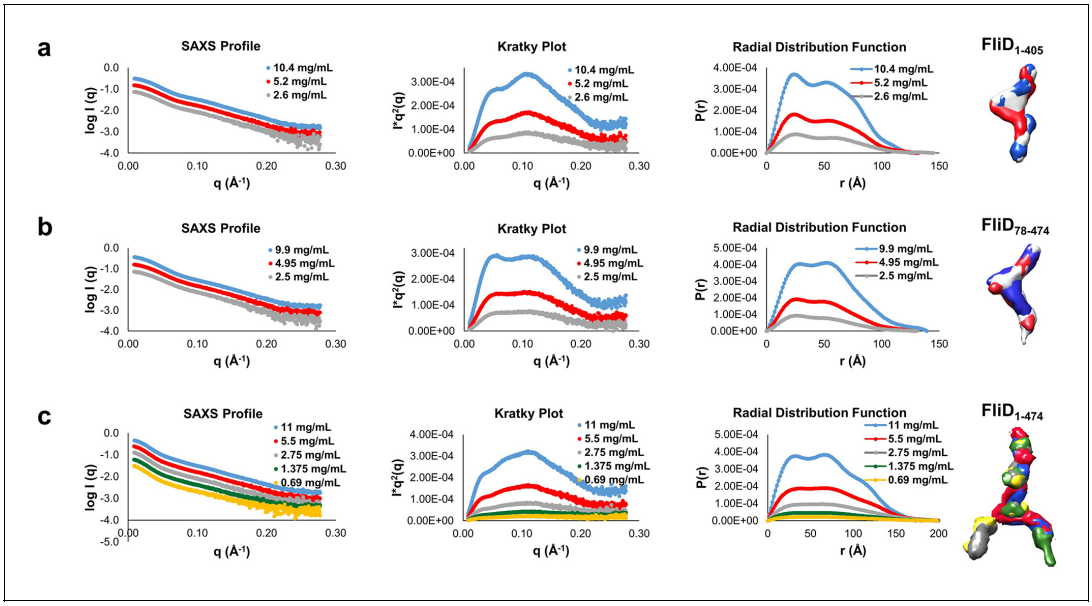

Figure 6. Small angle X-ray scattering (SAXS) data of $FliD_{1–405}$, $FliD_{78–474}$ and $FliD_{1–474}$. Log-scale intensity SAXS profiles, Kratky Plot ($I \times q^2$ *versus* q), radial distribution function calculated by GNOM and SAXS envelopes calculated by DAMMIF are shown for: (**a**) $FliD_{1–405}$ at 10.4 mg/mL (blue), 5.2 mg/mL (red) and 2.6 mg/mL (grey); (**b**) $FliD_{78–474}$ at 9.9 mg/mL (blue), 4.95 mg/mL (red) and 2.5 mg/mL (grey); and (**c**) $FliD_{1–474}$ at 11 mg/mL (blue), 5.5 mg/mL (red), 2.7 mg/mL (grey), 1.38 mg/mL (green) and 0.69 mg/mL (yellow).

DOI: 10.7554/eLife.18857.014

The following figure supplement is available for figure 6:

Figure supplement 1. Analytical ultracentrifugation (AUC) analysis of $FliD_{1–474}$ at pH 11.0.

DOI: 10.7554/eLife.18857.015

of domain 1. The leg region, particularly residues C-terminal to the α helix observed in the crystal structure, is more disordered or less stable (***Figure 7a***). Residues linking head domain 1 to the leg helix display cooperative unfolding behavior as indicated by EX1 kinetics (***Weis et al., 2006***) that result in double isotopic envelopes (***Figure 7b***). The $FliD_{78–405}$ protein used in these experiments was folded properly as shown by circular dichroism, as were all other FliD protein fragments that we produced (***Figure 7—figure supplement 1***). When mapped to our crystal structure of $FliD_{78–405}$, the degree of H/D exchange over time on the peptide level corresponds to the degree of conformational stability on the residue level (***Figure 7c***). When we used a difference plot to compare the extent of H/D exchange of full length $FliD_{1–474}$ with that of $FliD_{78–405}$, we observed that residues 165–225 exhibit relatively greater stability in $FliD_{78–405}$ (***Figure 8a***). Within this stretch of residues in head domain 2 are those residues, 165–171, which form the interface between the two head region domains in the hexameric complex (***Figure 8b***). We observed an additional region of relative stabilization for residues 298–324, part of which, residues 300–308, correspond to the β strand replacement in the opposing head region domain 1 that drives dodecamer formation of $FliD_{78–405}$ (***Figure 8a***). Kratky plots calculated from SAXS data of full-length $FliD_{1–474}$ at pH 11, which is monomeric under these conditions (***Figure 6—figure supplement 1***), confirms the overall flexible nature of this protein. Accordingly, heterogeneous molecular envelopes calculated from SAXS data collected at different concentrations of $FliD_{1–474}$ also exhibit significant conformational flexibility (***Figure 6c***).

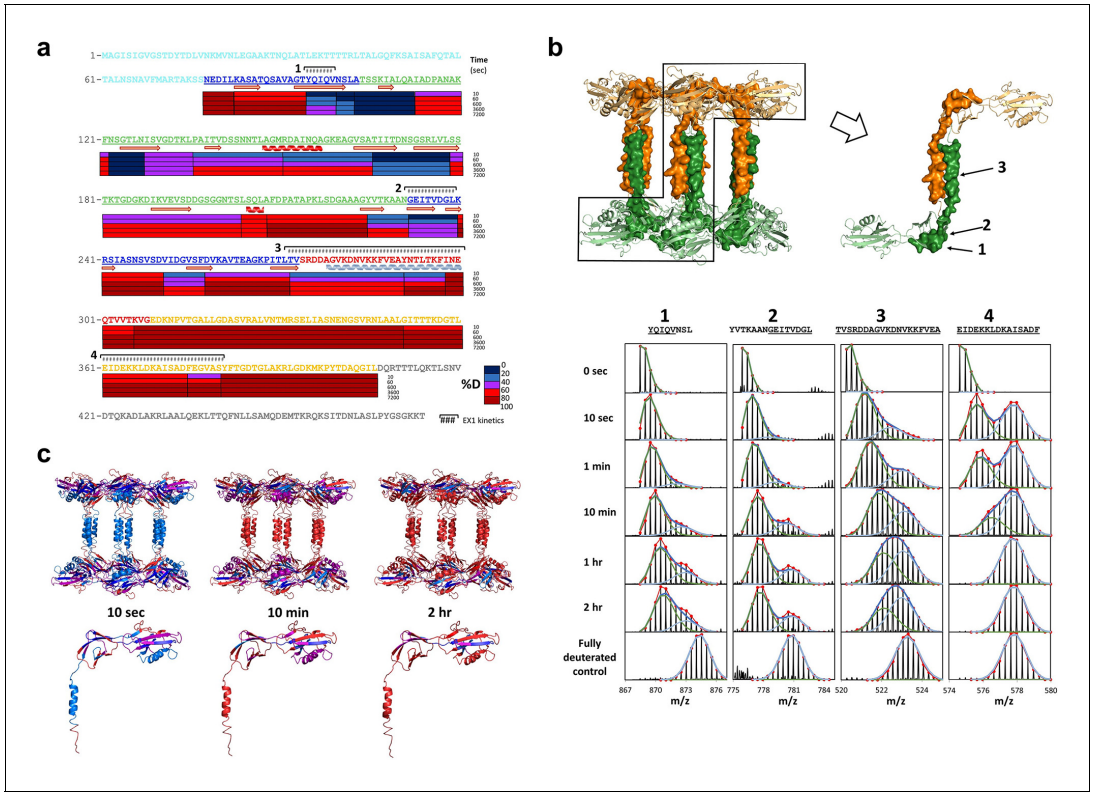

Figure 7. Regions of *Pseudomonas* FliD outside of the head domains and initial leg helix are highly dynamic. (**a**) Hydrogen/deuterium exchange analysis of $FliD_{78–405}$. Percent deuteration (%D) heat map is shown. Peptides exhibiting EX1 kinetics are indicated. (**b**) Mass spectra of four FliD peptides exhibit double isotopic envelopes characteristic of EX1 kinetics (*below*). Three of these peptides are mapped to the crystal structure (*above*; FliD hexamers are in green and gold). (**c**) Conformational stability as determined by hydrogen/deuterium exchange mapped to the crystal structure of $FliD_{78–405}$ using the same color coding for %D as shown in (**a**).

DOI: 10.7554/eLife.18857.016

The following figure supplement is available for figure 7:

Figure supplement 1. Circular dichroism analysis of FliD variants.

DOI: 10.7554/eLife.18857.017

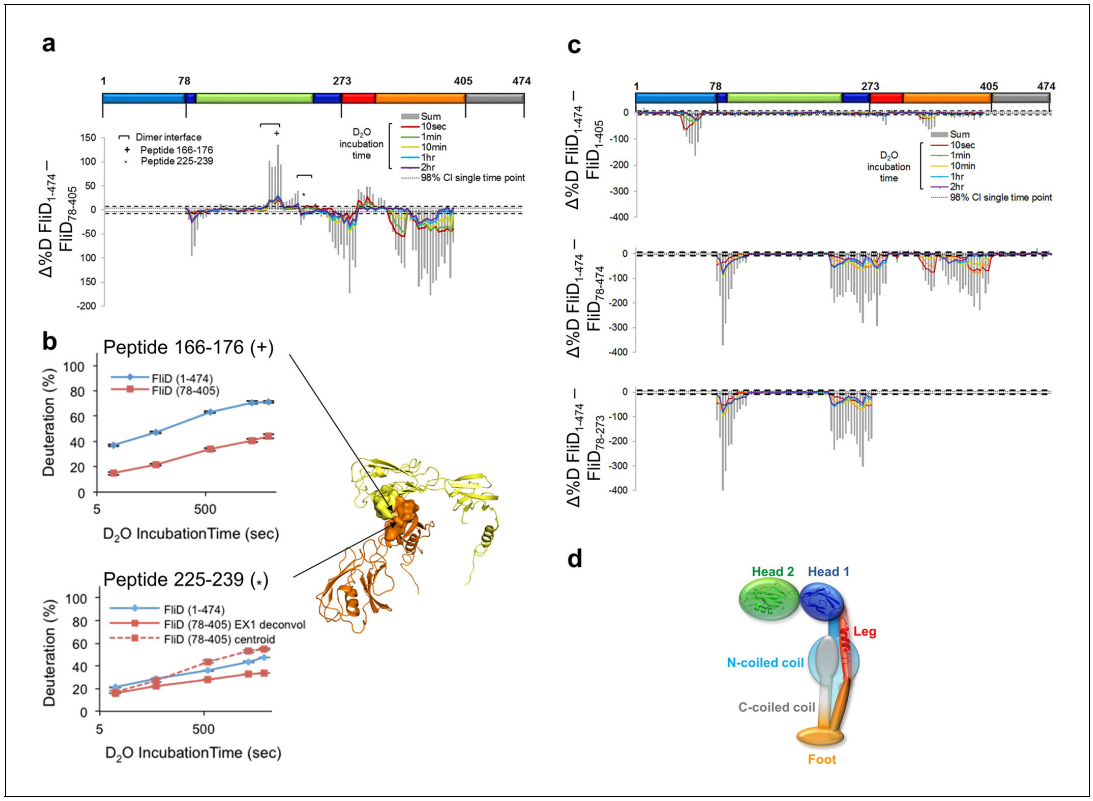

Figure 8. Interaction of *Pseudomonas* FliD regions. (**a**) Difference plot of hydrogen/deuterium exchange data from full length $FliD_{1–474}$ and the crystallized fragment, $FliD_{78–405}$. (**b**) Hydrogen/deuterium exchange for peptides corresponding to residues 166–176 (*top*, marked by + in (**a**) and (**b**)) and residues 225–239 (*bottom*, marked by * in (**a**) and (**b**)). Positions of peptides 166–176 and 225–239 in the $FliD_{78–405}$ crystal structure (*right*). (**c**) Difference plots of hydrogen/deuterium exchange data from full length $FliD_{1–474}$ and the fragments missing only the C-terminal coiled coil, $FliD_{1–405}$, only the N-terminal coiled coil, $FliD_{78–474}$, or both the N- and C-terminal coiled coils and the leg domain, $FliD_{78–273}$ (*top, middle and bottom, respectively*). (**d**) Schematic model of the FliD monomeric subunit showing the N-terminal coiled coil stabilizing the head 1 and foot domains and also interacting with the C-terminal coiled coil.

DOI: 10.7554/eLife.18857.018

The following figure supplements are available for figure 8:

Figure supplement 1. Hydrogen-deuterium exchange-mass spectrometry analysis of FliD variants.

DOI: 10.7554/eLife.18857.019

Figure supplement 2. Analytical ultracentrifugation (AUC) analysis of $FliD_{1–474}$ at 4 μM.

DOI: 10.7554/eLife.18857.020

Figure supplement 3. FliD intrinsic disorder analysis.

DOI: 10.7554/eLife.18857.021

Multiple regions of FliD interact with one another

To gain further insight to the dynamics and interactions of the different regions of FliD, we performed HDX-MS experiments with the remaining *Pseudomonas* FliD fragments that we had generated (***Figure 1a***, ***Figure 1—figure supplement 1***). HDX-MS heat maps show the overall high degree of flexibility of FliD regions outside the head domain (***Figure 8—figure supplement 1***), and difference plots of FliD truncations in comparison to the full length $FliD_{1–474}$ indicate that the head region, and more specifically head region domain 1, is stabilized by FliD regions outside of the head region (***Figure 8c***). Indeed, the N-terminal coiled coil is responsible for this stabilization of head region domain 1, in addition to stabilization of residues between the leg region α helix and the C-terminal coiled coil (***Figure 8c***). Finally, the C-terminal coiled coil predominantly stabilizes residues in the N-terminal coiled coil (***Figure 8c***). The stabilization of one FliD region by another is most likely to be direct and intramolecular, rather than allosteric and intermolecular, as the full-length protein $FliD_{1–474}$ adopts predominantly monomeric species under the conditions that we used for HDX-MS analysis

(*Figure 8—figure supplement 2*). This leads to a transient structural model of the entire FliD monomer subunit (*Figure 8d*) in which the N-terminal coiled coil bridges the head and foot regions and is itself pinned to these structural elements by the C-terminal coiled coil. Notably, none of the flexible regions of FliD, save the C-terminal 20 residues, are consistently predicted by sequence analysis to be intrinsically disordered (*Figure 8—figure supplement 3*); rather, they are inherently capable of adopting a limited number of conformations required to be in an 'on-state' (actively chaperoning and sorting a FliC protein) or an 'off-state' (engaging only structured and previously positioned FliC proteins).

Discussion

At the gross structural level, our studies show that the oligomeric states differ between FliD protein assemblies in diverse bacteria. *Salmonella* has long served as the model for bacterial flagellum structure and function. Since *Salmonella* FliD performs its native flagellar capping function as a pentamer (*Imada et al., 1998*; *Maki et al., 1998*; *Vonderviszt et al., 1998*; *Yonekura et al., 2000*), it could reasonably be assumed that all FliD proteins form pentamers at the distal ends of all bacterial flagella. We found that *Pseudomonas* FliD instead forms hexamers both in crystals and in solution. Additionally, we showed that *Pseudomonas* FliD constrained to its hexameric state by inter-subunit disulfide bonds is functional in vivo, resulting in the formation of flagella and swimming motility. Conversely, *Salmonella* FliD that assembles as pentamers does not allow flagellar formation and swimming motility in *Pseudomonas* bacteria.

Much like cryo-EM studies of flagellar filaments from diverse bacteria unequivocally showed that the number of protofilaments ranges, at least, from 11 in *Salmonella* (*Yonekura et al., 2003*) to seven in *Campylobacter* (*Galkin et al., 2008*), our structural analyses show that the proteins that cap these filaments also vary in their oligomeric states. The end of the *Salmonella* filament exhibits a non-planar surface with five indentations (*Yonekura et al., 2000*) into which the five legs of the corresponding FliD pentamer have been modeled (*Maki-Yonekura et al., 2003*). Although no structure of the *Pseudomonas* filament has been determined even at low resolution, our hexameric FliD structure suggests that it may incorporate an even greater number of protofilaments than does the *Salmonella* filament. This would allow the formation of an additional molecular cavity on the distal end of FliD that accommodates its unique capping protein hexamer. Indeed, *Pseudomonas* flagellar filaments have been found to be macroscopically different from those of *Salmonella* (*Shibata et al., 2005*).

At 2.2 Å resolution, our crystal structure reveals several previously unknown structural features of FliD that are likely to be critical to its function. First, each one of the six FliD head regions that appear as discreet lobes when visualized by EM analysis is actually composed of the first and second domains of neighboring monomer subunits, as opposed to both domains belonging to the same subunit. This is likely the case for FliD oligomers from diverse bacteria, including *Salmonella* FliD for which cryo-EM analyses showed five head region lobes (*Maki-Yonekura et al., 2003*; *Yonekura et al., 2000*, *2003*). Second, despite vanishingly low sequence similarity, each domain within the head region exhibits high structural similarity to the corresponding domains of other flagellar proteins, including the hook-filament junction protein/FlgK and flagellin/FliC. Thus, at least one protein domain from the proteins that occupy the distal ends of the hook (FlgK) and the cap (FliD) adopts a common structural fold, which may be required for and unique to their function at these related positions within the flagellum. This domain conservation among flagellar proteins confirms a previous study proposing a structural relationship of FliD to other flagellar proteins despite their low sequence similarities (*Vonderviszt et al., 1998*). This structural conservation suggests that a structurally similar cap complex may form at both hook and on the distal end. It also suggests that FliD may play a functional role earlier in the flagellar assembly process, prior to its known FliC sorting function. Notably, in mutants of *Salmonella* that lack filaments, FlgK (HAP1), FliD (HAP2) and FlgL (HAP3) form a layered structure at the distal end of the hook-basal body (*Homma and Iino, 1985*). In addition, the shared domain structure of portions of FliC and FliD suggests that the chaperoning activity of FliD could derive, at least in part, from its presentation of a like-structured template against which FliC subunits may fold prior to being positioned into the growing filament.

Owing to the conformational flexibility of FliD necessitated by its FliC sorting function, we still lack high-resolution structural information for certain regions of this protein. However, using a

number of biophysical methods, we found that molecular determinants outside of the conformationally stable head regions control FliD oligomerization. Previous analysis of a trypsinized fragment of *Salmonella* FliD that lacks the N-terminal 42 residues and C-terminal 51 residues, which is similar to the *Pseudomonas* $FliD_{78–405}$ protein that we crystallized, showed that this fragment can form pentamers but not decamers in solution and dissociates into smaller oligomers at low temperatures (**Vondervisztet al., 1998**). This suggests that determinants outside of the head regions of FliD proteins of diverse bacteria control their oligomeric states. Accordingly, we showed that FliD, when constrained to its hexameric state by disulfide bonds formed between neighboring head domain subunits, is fully functional in vivo. Thus,conformational flexibility in or relative repositioning of the head regions are not functional requirements of FliD but flexibility in regions outside of the head regions undoubtedly is. Considering that inhibiting protein–protein interfaces with small molecules remains a major technical challenge (**Arkin et al., 2014**), the dependence of FliD oligomeric assembly on its flexible regions enhances the prospects of developing small molecule inhibitors of FliD oligomerization, and consequently of flagellar function, as a novel class of antibiotic agents.

Materials and methods

Plasmids

For crystallization, the coding sequence optimized for expression in *E. coli* of $FliD_{78–405}$ from the PAO1 strain of *P. aeruginosa* was synthesized and cloned into the pET-28b vector (Novagen) with the inclusion of an N-terminal His_6-tag followed by a tobacco etch virus (TEV) protease recognition site. A $FliD_{78–405}$ mutant encoding four leucine to methionine mutations at positions L135, L239, L347 and L350 ($FliD_{78–405}/L_4$-M_4) was synthesized and likewise cloned into the pET-28b vector with an N-terminal His_6-tag. For all other experiments, $FliD_{78–405}$, full-length FliD ($FliD_{1\ –474}$), head domain-only FliD ($FliD_{78\ –273}$), and FliD lacking the N-terminal ($FliD_{78\ –474}$) or C-terminal ($FliD_{1\ –405}$) coiled-coil domains were codon-optimized for expression in *E. coli* and cloned into pGEX5x2 in frame with an N-terminal GST-tag followed by a TEV protease site. To obtain a stable hexameric full-length FliD mutant ($FliD_{1\ –474(I167C/D253C)}$), two residues (I167 and D253) located at the interface between neighboring head domains were mutated to cysteine residues in wildtype $FliD_{1–474}$.

Recombinant protein expression and purification

All FliD constructs from the *P. aeruginosa* PAO1 strain were expressed in LB medium for 4 hr at 37°C in *E. coli* BL21(DE3)pLysS cells after induction with 1 mM IPTG at an OD_{600nm} of 0.6. Selenomethionine (SeMet)-labeled $FliD_{78\ –405}/L_4$-M_4 was produced using metabolic inhibition of methionine biosynthesis (**Van Duyne et al., 1993**) and growth in M9 medium containing 60 mg/L SeMet as the sole source of methionine for 6 hr after induction with 1 mM IPTG. Cells were harvested (5000 g for 15 min) and lysed in PBS including 5 mM β-mercaptoethanol by sonication. For crystallization of His-tagged $FliD_{78\ –405}$ and His-tagged $FliD_{78\ –405}/L_4$-M_4,the soluble fraction was purified using HisPur NiNTA Resin (Thermo Scientific). The protein was further purified by size exclusion chromatography (Superdex 200 10/300 GL, GE Healthcare) in PBS followed by anion exchange chromatography (MonoQ 5/50 GL, GE Healthcare). For crystallization the protein was dialyzed into 30 mM Tris pH 8.0, 80 mM sodium chloride and concentrated to approximately 13 mg/mL. FliD-GST-fusion constructs were purified using a Glutathione Sepharose (BioVision) column. Following 16 hr digestion with TEV protease, the GST tag was removed by Glutathione Sepharose and TEV was removed by NiNTA (Thermo Scientific) chromatography. Cleaved FliD constructs were further purified using size exclusion (Superdex 200 10/300 GL, GE Healthcare) in PBS followed by anion exchange chromatography (MonoQ 5/50 GL, GE Healthcare) using 20 mM CHES pH 9.0 and a linear salt gradient from 0 to 1 M NaCl over 12 min.

Protein crystallization

Crystals of $FliD_{78\ –405}$ obtained in 0.25 M L-Arginine, 0.1 M Tris/HCl pH 8.0, 8% PGA diffracted poorly and were subsequently used for random microseeding matrix screening (rMMS) (**D'Arcy et al., 2007**). Improved crystals of $FliD_{78\ –405}$ were grown in 0.8 M NaK Tartrate, 0.1 M Hepes pH 7.5 and diffracted to 2.2 Å. Crystals of SeMet-labeled $FliD_{78\ –405}/L_4$-M_4 were also obtained by employing rMMS with the initial, poorly diffracting crystals of $FliD_{78\ –405}$, which resulted

in $FliD_{78\ -405}/L_4$-M_4 crystals grown in 1.5 M ammonium sulfate, 0.1 M Tris pH 8.5, 10% glycerol diffracting to 3.6 Å (anomalous signal cuttoff). Crystals were harvested and flash cooled in liquid nitrogen in mother liquor supplemented with 25% to 30% glycerol as cryo-protectant.

X-ray diffraction data processing, structure determination and refinement

X-ray diffraction data for the SeMet-labeled $FliD_{78\ -405}/L_4$-M_4 crystal were collected using a Dectris 6M PILATUS detector on the 12–2 beamline at the Stanford Synchrotron Radiation Lightsource, SSRL, processed using XDS (***Kabsch, 2010b***), scaled in AIMLESS (***Evans and Murshudov, 2013***; ***Winn et al., 2011***), and phases obtained using the SSRL multi-wavelength anomalous dispersion (MAD) script by A. Gonzalez with SHELX options based on a script by Qingping Xu, including the programs SHELX (***Schneider and Sheldrick, 2002***), SOLVE (***Terwilliger and Berendzen, 1999***) and RESOLV (***Terwilliger, 2000***). The initial $FliD_{78\ -405}/L_4$-M_4 model was improved manually by rebuilding the peptide chain backbone in Coot (***Emsley and Cowtan, 2004***) and refining using Phenix (***Adams et al., 2010***). Diffraction data for native, wildtype $FliD_{78\ -405}$ were collected using a MARmosaic 300 CCD detector on the 23ID-B beamline at the Advanced Photon Source, Argonne National Laboratory, APS, and processed using XDS (***Kabsch, 2010b***) and XSCALE (***Kabsch, 2010a***). The partially built and refined SeMet-$FliD_{78\ -405}/L_4$-M_4 model was used as a molecular replacement model for phasing the native $FliD_{78–405}$ data using Phaser (***McCoy et al., 2007***). The initial native $FliD_{78–405}$ model was build using Autobuild and improved by manual model rebuilding in Coot (***Emsley and Cowtan, 2004***) and by iterative rounds of refinement using Phenix (***Adams et al., 2010***).

Mass spectrometry

$FliD_{78–405}$ crystals were crosslinked using 2% formaldehyde, harvested and washed in mother liquor, dissolved in water and the crosslinking reversed by heating the samples to 95°C for 20 min. The samples were analyzed by liquid chromatography (LC)-electrospray ionization (ESI)-mass spectrometry (MS) using a gradient of mobile phase A (0.1% formic acid in water) and mobile phase B (0.1% formic acid in acetonitrile) increasing from 0% B to 90% B in 20 min. The Accela LC System was attached to a LXQ linear ion trap mass spectrometer (Thermo Scientific). Raw MS data were analyzed using Xcalibus Qual Browser (Thermo Scientific) and deconvoluted using BioWorks (Thermo Scientific, Waltham, MA).

Circular dichroism

10 µM FliD protein in 10 mM sodium phosphate pH 7.0 was used to record a spectrum ranging from 190 nm to 260 nm at 15°C. CD melting curves were analyzed at 222 nm or 205 nm by increasing the temperature by 1°C per minute starting at 15°C using a JASCO J810 CD instrument according to the manufacturer's instructions.

Electron microscopy

An aliquot of a $FliD_{78–405}$ protein sample was negatively stained with 2% (weight/volume) uranyl acetate and imaged using a Tecnai F20 (FEI) electron microscope operating at 120 keV. Approximately 3500 particles were selected from 70 micrographs and used to generate class averages in EMAN2 (***Tang et al., 2007***). Six classes were generated, and ***Figure 3a*** shows the single largest class.

Small angle X-ray scattering (SAXS)

Small angel x-ray scattering data were collected using a dual Pilatus 100K-S SAXS/WAXS detector at beamline G-1 of the Macromolecular Diffraction Facility at the Cornell High Energy Synchrotron Source (MacCHESS). Scattering was measured in 30 mM Tris pH 8.0, 80 mM NaCl of $FliD_{78–405}$ at 10.7 mg/mL, 5.4 mg/mL and 2.7 mg/mL, of $FliD_{78–273}$ at 1.34 mg/mL, 0.67 mg/mL and 0.335 mg/mL, of $FliD_{1–405}$ at 10.4 mg/mL, 5.2 mg/mL and 2.6 mg/mL, of $FliD_{78–474}$ at 9.9 mg/mL, 4.95 mg/mL and 2.6 mg/mL and of $FliD_{1–474(I167C/D253C)}$ at 9.75 mg/ml, 4.88 mg/ml and 2.44 mg/ml. Scattering of monomeric full-length $FliD_{1–474}$ at 11 mg/mL, 5.5 mg/mL, 2.75 mg/mL, 1.38 mg/mL and 0.69 mg/mL was measured in 20 mM CAPS pH 11.0, 80 mM NaCl. The SAXS data were processed using the BioXTAS RAW software (***Nielsen et al., 2009***) and radial distribution functions calculated using GNOM (***Svergun, 1992***). Molecular envelopes were generated using GASBOR (***Svergun et al., 2001***) and

DAMMIF (**Lammie et al., 2007**). FoXS (**Schneidman-Duhovny et al., 2010**) was used to verify the calculated intensity plots of the structures of the head domain $FliD_{78–273}$ and the dodecameric $FliD_{78–405}$. The X-ray crystal structures of $FliD_{78–273}$ and $FliD_{78–405}$ were superimposed onto the envelopes.

Hydrogen/deuterium exchange-mass spectrometry

The coverage maps for $FliD_{1–474}$ and $FliD_{78–405}$ were obtained from undeuterated controls as follows: 3.5 µL of ~40 µM FliD in 30 mM TrisHCl, 150 mM NaCl pH 8.0 was diluted with 31.5 µL of the same buffer at room temperature followed by the addition of 100 µL of ice cold quench (100 mM Phosphate buffer, 1.5 M Guanidine-HCl, pH 2.4). The quenched samples were injected into a Waters HDX nanoAcquity UPLC (Waters, Milford, MA) with in-line pepsin digestion (Waters Enzymate BEH pepsin column). Peptic fragments were trapped on an Acquity UPLC BEH C18 peptide trap and separated on an Acquity UPLC BEH C18 column. A 7 min, 5% to 35% acetonitrile (0.1% formic acid) gradient was used to elute peptides directly into a Waters Synapt G2 mass spectrometer (Waters, Milford, MA). MS^E data were acquired with a 20 to 30 V ramp trap CE for high energy acquisition of product ions as well as continuous lock mass (Leu-Enk) for mass accuracy correction. Peptides were identified using the ProteinLynx Global Server 2.5.1 (PLGS) from Waters. Further filtering of 0.3 fragments per residues was applied in DynamX.

For each construct, the HD exchange reactions were performed as follows: 3.5 µL of ~40 µM FliD in 30 mM TrisHCl, 150 mM NaCl pH 8.0 was incubated in 31.5 µL of 30 mM TrisDCl, 99.99% D_2O, pD 8.0, 150 mM NaCl. All reactions were performed at 25°C. Prior to injection, deuteration reactions were quenched at various times (10 s, 1 min, 10 min, 1 hr and 2 hr) with 100 µL of 100 mM Phosphate buffer, 1.5 Guanidine-HCl, pH 2.4. Back exchange correction was performed against fully deuterated controls acquired by incubating 3.5 µL of 40 µM $FliD_{1–474}$ in 31.5 µL 30 mM TrisDCl, 99.99% D_2O, pD 8.0, 150 mM NaCl containing 6 M deuterated Guanidine DCl for 2 hr at 25°C prior to quenching (without guanidine HCl). All deuteration time points and controls were acquired in triplicates.

The deuterium uptake by the identified peptides through increasing deuteration time and for the fully deuterated control was determined using Water's DynamX 2.0 software. The normalized percentage of deuterium uptake (%D) at an incubation time t for a given peptide was calculated as follows:

$$\%D = \frac{100 \cdot (m_t - m_0)}{m_f - m_0}$$

With m_t the centroid mass at incubation time t, m_0 the centroid mass of the undeuterated control, and m_f the centroid mass of the fully deuterated control. Heat maps and percent deuteration difference plots ($\Delta\%D$) were generated using the percent deuteration calculated. Confidence intervals for the $\Delta\%D$ plots were determined using the method outlined by **Houde et al. (2011)**, adjusted to percent deuteration using the fully deuterated controls. Confidence intervals (98%) were plotted on the $\Delta\%D$ plots as horizontal dashed lines. EX1 type cooperative unfolding was analyzed using HX-Express2 (**Guttman et al., 2013**).

Determination of peptide coverage of $FliD_{1–474(I167C/D253C)}$ under reducing and non-reducing conditions

Coverage maps of $FliD_{1–474(I167C/D253C)}$ in the presence and absence of reducing agent were obtained similarly as above except for the following: 3 µL of 66 µM $FliD_{1–474(I167C/D253C)}$ were incubated for 2 hr with 15 µL of 8 M Guanidine-HCl and 2 µL of 1 M TCEP (reducing conditions) or 2 µL H_2O (non-reducing conditions). Subsequently, 180 µL of quench buffer (100 mM potassium buffer, pH 2.4) was added and the mixture immediately injected into the Waters HDX nanoAcquity UPLC. The remainder of the workflow, MS method, peptide identification and coverage map determination was unchanged. In addition, Biopharmalynx 1.3.5 (Waters) was used to search for and to identify disulfide-bridged peptides. A filter of 15% b/y ions identified was applied. The search was performed both in the context of the expected C167–C253 disulfide bridge and forthe C167–C167 and C253–C253 disulfide bridges as negative controls.

Analytical ultracentrifugation

The oligomeric states of $FliD_{78–405}$, $FliD_{78–273}$ and $FliD_{1–474}$ in buffers containing 30 mM Tris, 80 mM NaCl, pH 8.0 or 20 mM sodium citrate, 80 mM NaCl, pH 5.0 respectively, were analyzed by sedimentation velocity using a Beckman-Coulter XL-I analytical ultracentrifuge equipped with a 4- or 8-hole An-60Ti Rotor at 20˚C. SedenTerp (http://sednterp.unh.edu) was used to calculate protein partial specific volumes and solvent densities and viscosities from the protein amino acid sequences and buffer compositions. For sedimentation velocity measurements, samples of 295 µM (pH 8.0) or 325 µM (pH 5.0) $FliD_{78–405}$, 124 µM $FliD_{78–273}$, and 168 µM $FliD_{1–474}$ were prepared in each buffer. $FliD_{1–474}$ was also analyzed by AUC at a low concentration of 4 µM in 30 mM Tris, 80 mM NaCl, pH 8.0 and at a concentration of 43 µM at high pH in 20 mM CAPS, 80 mM NaCl, pH 11.0. After exhaustive dialysis to ensure chemical equilibrium, the samples were loaded into cells equipped with 2-hole charcoal-filled epon centerpieces (either 1.2 or 0.3 mm path length) with sapphire windows. Prior to centrifugation, samples were equilibrated in the rotor for at least 2 hr at the desired experimental temperature. Centrifugation was performed at 50,000 ($FliD_{78–273}$), 40,000 ($FliD_{1–474}$) or 30,000 ($FliD_{78–273}$) rpm and scans were acquired at 280 nm. The resulting data were analyzed using DCDT+ version 2.2.1 (**Philo, 2006**; **Stafford, 1997**, **1992**) to determine the number of species, their sedimentation coefficients, and their fractional contributions to the species populations. All sedimentation coefficients were corrected to $s_{20,w}$ values.

Chemical crosslinking

Approximately 0.4 mg/mL of protein in 20 mM Hepes pH 8.0, 10 mM sodium chloride was crosslinked using 20 mM 1-ethyl-3-(3-dimethylaminopropyl)carbodiimide hydrochloride (EDC) and 20 mM N-hydroxysuccinimide (NHS) in 20 mM sodium phosphate, pH 7.0, 150 mM NaCl for various time points. The reaction was stopped by the addition of 0.5 M Tris-HCl pH 8.0 to a final concentration of 0.25 M. The products were analyzed on NuPAGE 3–8% Tris-Acetate gels (Life Technologies, Carlsabd, CA) or an Any kD Mini-PROTEAN TGX gels (BioRad) using a silver-staining kit (Thermo Scientific).

Complementation of *Pseudomonas aeruginosa* PAO1

Wildtype $fliD_{1474}$ and $fliD_{1474(I167C/D253C)}$ were cloned into pUCP20 and transformed by electroporation (**Cadoret et al., 2014**) into the Δ*fliD* transposon strain PW2975 (obtained from the Manoil Lab at the University of Washington), resulting in the strains $\Delta fliD/fliD_{1–474}$ and $\Delta fliD/fliD_{1–474(I167C/D253C)}$, respectively. Wildtype $fliD_{1–474}$ ($fliD_{1–474e}$) and full-length *fliD* from *Salmonella typhimurium* ($fliD_{StyFliDe}$) both with genes codon-optimized for *E. coli* expression were also transformed into PW2975 resulting in $\Delta fliD/fliD_{1–474e}$ and $\Delta fliD/fliD_{StyFliDe}$, respectively.

Swimming motility assays

Swimming motility assays of *Pseudomonas aeruginosa* strains were performed as described by **Ha et al. (2014)**.

Isolation of flagella and FliD detection

Pseudomonas aeruginosa PAO1 was grown overnight in LB liquid culture, cells were spun down and resuspended in PBS. Flagella were sheared off the cells by passing the suspension through a 23 gauge needle approximately 25 times. After centrifugation, the supernatant containing flagella was concentrated, proteins separated by SDS-PAGE and analyzed by Western blot using anti-FliD scFv-Fc SH1579-B7 and an anti-human-IgG-HRP conjugate secondary antibody.

Generation of anti-FliD antibodies

Human antibodies were generated as described by **Frenzel et al. (2014)**. In brief, recombinant head region only $FliD_{78\ –273}$ was immobilized on Costar High Binding plates and incubated with the Hyperphage packaged human antibody gene libraries HAL9/10 (**Kügler et al., 2015**) for negative selection. The non-binding scFv phages were incubated with recombinant full-length $FliD_{1\ –474}$ to select binders specific for the leg region of FliD. In total, three panning rounds were performed and monoclonal antibodies were identified as described by **Frenzel et al. (2014)**. The antibody SH1579-B7

was recloned as an scFv-Fc (Yumab) with a human IgG1 Fc region and produced in mammalian cell culture as described by ***Jäger et al. (2013)***.

Intrinsic disorder

The sequence of the full-length FliD was submitted to twelve publicly available servers implementing different algorithms for protein disorder prediction. In all cases, we used the default parameters. The servers used were as follows: disEMBL (***Linding et al., 2003a***), GlobProt (***Linding et al., 2003b***), IUPred (***Dosztanyi et al., 2005***), RONN (***Yang et al., 2005***), DisPro (***Cheng et al., 2005***), PONDR (***Romero et al., 2001***), Spine-D (***Zhang et al., 2012***), OnD-CRF (***Wang and Sauer, 2008***), Foldindex (***Prilusky et al., 2005***), MFDp (***Mizianty et al., 2010***), MFDp2 (***Mizianty et al., 2010***), and MD2 (***Kozlowski and Bujnicki, 2012***). Averaging of the results gave all servers equal weight.

Accession code

Coordinates and structure factors have been deposited in the Protein Data Bank under accession code 5FHY.

Acknowledgements

We thank the staff of the Stanford Synchrotron Radiation Lightsource (SSRL) beamline 12-2, SLAC National Accelerator Laboratory, San Francisco, USA, of the Advanced Photon Source (APS) GM/CA CAT beamline 23-ID-B, Argonne National Laboratory, Illinois, USA and of the beamline G-1 of the Macromolecular Diffraction facility at Cornell High Energy Synchrotron Source (MacCHESS), Ithaca, USA for their support. This work is supported in part by the University of Maryland Baltimore, School of Pharmacy Mass Spectrometry Center (SOP1841-IQB2014).

Additional information

Competing interests

EHE: Reviewing editor, *eLife*. The other authors declare that no competing interests exist.

Funding

Funder	Grant reference number	Author
National Center for Research Resources	NIH S10 RR15899	Dorothy Beckett

The funders had no role in study design, data collection and interpretation, or the decision to submit the work for publication.

Author contributions

SP, Designed the project, Performed experiments, Analysis of data, Writing the manuscript, Conception and design, Acquisition of data, Analysis and interpretation of data, Drafting or revising the article; DD, Performed experiments, Analysis of data, Reviewed the manuscript, Acquisition of data, Analysis and interpretation of data; DAB, KD, PLW, Analysis of data, Analysis and interpretation of data; XY, MH, DB, Performed experiments, Analysis of data, Acquisition of data, Analysis and interpretation of data; SH, Performing experiments, Acquisition of data; AV, AF, Intrinsic disorder prediction, Analysis and interpretation of data; EHE, Performed experiments, Analysis of data, Analysis and interpretation of data; EJS, Designed the project, Analysis of data, Writing the manuscript, Conception and design, Analysis and interpretation of data, Drafting or revising the article

Author ORCIDs

Sandra Postel, http://orcid.org/0000-0002-6717-1870
Edward H Egelman, http://orcid.org/0000-0003-4844-5212
Eric J Sundberg, http://orcid.org/0000-0003-0478-3033

Additional files

Major datasets

The following dataset was generated:

Author(s)	Year	Dataset title	Dataset URL	Database, license, and accessibility information
Postel S, Bonsor D, Diederichs K, Sundberg EJ	2016	Crystal structure of FliD (HAP2) from Pseudomonas aeruginosa PAO1	http://www.rcsb.org/pdb/explore/explore.do?structureId=5FHY	Publicly available at the RCSB Protein Data Bank (accession no. 5FHY)

References

Adams PD, Afonine PV, Bunkóczi G, Chen VB, Davis IW, Echols N, Headd JJ, Hung LW, Kapral GJ, Grosse-Kunstleve RW, McCoy AJ, Moriarty NW, Oeffner R, Read RJ, Richardson DC, Richardson JS, Terwilliger TC, Zwart PH. 2010. PHENIX: a comprehensive Python-based system for macromolecular structure solution. *Acta Crystallographica Section D Biological Crystallography* **66**:213–221. doi: 10.1107/S0907444909052925

Allen-Vercoe E, Woodward MJ. 1999. The role of flagella, but not fimbriae, in the adherence of Salmonella enterica serotype Enteritidis to chick gut explant. *Journal of Medical Microbiology* **48**:771–780. doi: 10.1099/00222615-48-8-771

Arkin MR, Tang Y, Wells JA. 2014. Small-molecule inhibitors of protein-protein interactions: progressing toward the reality. *Chemistry & Biology* **21**:1102–1114. doi: 10.1016/j.chembiol.2014.09.001

Arora SK, Neely AN, Blair B, Lory S, Ramphal R. 2005. Role of motility and flagellin glycosylation in the pathogenesis of Pseudomonas aeruginosa burn wound infections. *Infection and Immunity* **73**:4395–4398. doi: 10.1128/IAI.73.7.4395-4398.2005

Arora SK, Ritchings BW, Almira EC, Lory S, Ramphal R. 1998. The Pseudomonas aeruginosa flagellar cap protein, FliD, is responsible for mucin adhesion. *Infection and Immunity* **66**:1000–1007.

Berg HC. 2003. The rotary motor of bacterial flagella. *Annual Review of Biochemistry* **72**:19–54. doi: 10.1146/annurev.biochem.72.121801.161737

Bergfors T. 2003. Seeds to crystals. *Journal of Structural Biology* **142**:66–76. doi: 10.1016/S1047-8477(03)00039-X

Black RE, Levine MM, Clements ML, Hughes TP, Blaser MJ. 1988. Experimental Campylobacter jejuni infection in humans. *Journal of Infectious Diseases* **157**:472–479. doi: 10.1093/infdis/157.3.472

Cadoret F, Soscia C, Voulhoux R. 2014. Gene transfer: transformation/electroporation. *Methods in Molecular Biology* **1149**:11–15. doi: 10.1007/978-1-4939-0473-0_2

Cheng J, Sweredoski MJ, Baldi P. 2005. Accurate prediction of protein disordered regions by mining protein structure data. *Data Mining and Knowledge Discovery* **11**:213–222. doi: 10.1007/s10618-005-0001-y

Craig DB, Dombkowski AA. 2013. Disulfide by Design 2.0: a web-based tool for disulfide engineering in proteins. *BMC Bioinformatics* **14**:346. doi: 10.1186/1471-2105-14-346

D'Arcy A, Villard F, Marsh M. 2007. An automated microseed matrix-screening method for protein crystallization. *Acta Crystallographica Section D Biological Crystallography* **63**:550–554. doi: 10.1107/S0907444907007652

Dosztányi Z, Csizmok V, Tompa P, Simon I. 2005. IUPred: web server for the prediction of intrinsically unstructured regions of proteins based on estimated energy content. *Bioinformatics* **21**:3433–3434. doi: 10.1093/bioinformatics/bti541

Duan Q, Zhou M, Zhu L, Zhu G. 2013. Flagella and bacterial pathogenicity. *Journal of Basic Microbiology* **53**:1–8. doi: 10.1002/jobm.201100335

Emsley P, Cowtan K. 2004. Coot: model-building tools for molecular graphics. *Acta Crystallographica Section D Biological Crystallography* **60**:2126–2132. doi: 10.1107/S0907444904019158

Evans PR, Murshudov GN. 2013. How good are my data and what is the resolution? *Acta Crystallographica Section D Biological Crystallography* **69**:1204–1214. doi: 10.1107/S0907444913000061

Frenzel A, Kügler J, Wilke S, Schirrmann T, Hust M. 2014. Construction of human antibody gene libraries and selection of antibodies by phage display. *Methods in Molecular Biology* **1060**:215–243. doi: 10.1007/978-1-62703-586-6_12

Galkin VE, Yu X, Bielnicki J, Heuser J, Ewing CP, Guerry P, Egelman EH. 2008. Divergence of quaternary structures among bacterial flagellar filaments. *Science* **320**:382–385. doi: 10.1126/science.1155307

Guttman M, Weis DD, Engen JR, Lee KK. 2013. Analysis of overlapped and noisy hydrogen/deuterium exchange mass spectra. *Journal of the American Society for Mass Spectrometry* **24**:1906–1912. doi: 10.1007/s13361-013-0727-5

Ha DG, Kuchma SL, O'Toole GA. 2014. Plate-based assay for swimming motility in Pseudomonas aeruginosa. *Methods in Molecular Biology* **1149**:59–65. doi: 10.1007/978-1-4939-0473-0_7

Haiko J, Westerlund-Wikström B. 2013. The role of the bacterial flagellum in adhesion and virulence. *Biology* **2**:1242–1267. doi: 10.3390/biology2041242

Homma M, Iino T. 1985. Locations of hook-associated proteins in flagellar structures of Salmonella typhimurium. *Journal of Bacteriology* **162**:183–189.
Houde D, Berkowitz SA, Engen JR. 2011. The utility of hydrogen/deuterium exchange mass spectrometry in biopharmaceutical comparability studies. *Journal of Pharmaceutical Sciences* **100**:2071–2086. doi: 10.1002/jps.22432
Imada K, Vonderviszt F, Furukawa Y, Oosawa K, Namba K. 1998. Assembly characteristics of flagellar cap protein HAP2 of Salmonella: decamer and pentamer in the pH-sensitive equilibrium. *Journal of Molecular Biology* **277**:883–891. doi: 10.1006/jmbi.1998.1662
Jones S, Thornton JM. 1996. Principles of protein-protein interactions. *PNAS* **93**:13–20. doi: 10.1073/pnas.93.1.13
Jäger V, Büssow K, Wagner A, Weber S, Hust M, Frenzel A, Schirrmann T. 2013. High level transient production of recombinant antibodies and antibody fusion proteins in HEK293 cells. *BMC Biotechnology* **13**:52. doi: 10.1186/1472-6750-13-52
Kabsch W. 2010a. Integration, scaling, space-group assignment and post-refinement. *Acta Crystallographica Section D Biological Crystallography* **66**:133–144. doi: 10.1107/S0907444909047374
Kabsch W. 2010b. Xds. *Acta Crystallographica Section D Biological Crystallography* **66**:125–132. doi: 10.1107/s0907444909047337
Kim JS, Chang JH, Chung SI, Yum JS. 1999. Molecular cloning and characterization of the Helicobacter pylori fliD gene, an essential factor in flagellar structure and motility. *Journal of Bacteriology* **181**:6969–6976.
Kozlowski LP, Bujnicki JM. 2012. MetaDisorder: a meta-server for the prediction of intrinsic disorder in proteins. *BMC Bioinformatics* **13**:111. doi: 10.1186/1471-2105-13-111
Krukonis ES, DiRita VJ. 2003. From motility to virulence: Sensing and responding to environmental signals in Vibrio cholerae. *Current Opinion in Microbiology* **6**:186–190. doi: 10.1016/S1369-5274(03)00032-8
Kügler J, Wilke S, Meier D, Tomszak F, Frenzel A, Schirrmann T, Dübel S, Garritsen H, Hock B, Toleikis L, Schütte M, Hust M. 2015. Generation and analysis of the improved human HAL9/10 antibody phage display libraries. *BMC Biotechnology* **15**:10. doi: 10.1186/s12896-015-0125-0
La Ragione RM, Sayers AR, Woodward MJ. 2000. The role of fimbriae and flagella in the colonization, invasion and persistence of Escherichia coli O78:K80 in the day-old-chick model. *Epidemiology and Infection* **124**:351–363. doi: 10.1017/S0950268899004045
Lammie D, Osborne J, Aeschlimann D, Wess TJ. 2007. Rapid shape determination of tissue transglutaminase using high-throughput computing. *Acta Crystallographica Section D Biological Crystallography* **63**:1022–1024. doi: 10.1107/S0907444907032933
Linding R, Jensen LJ, Diella F, Bork P, Gibson TJ, Russell RB. 2003a. Protein disorder prediction: implications for structural proteomics. *Structure* **11**:1453–1459. doi: 10.1016/j.str.2003.10.002
Linding R, Russell RB, Neduva V, Gibson TJ. 2003b. GlobPlot: Exploring protein sequences for globularity and disorder. *Nucleic Acids Research* **31**:3701–3708. doi: 10.1093/nar/gkg519
Maki S, Vonderviszt F, Furukawa Y, Imada K, Namba K. 1998. Plugging interactions of HAP2 pentamer into the distal end of flagellar filament revealed by electron microscopy. *Journal of Molecular Biology* **277**:771–777. doi: 10.1006/jmbi.1998.1663
Maki-Yonekura S, Yonekura K, Namba K. 2003. Domain movements of HAP2 in the cap-filament complex formation and growth process of the bacterial flagellum. *PNAS* **100**:15528–15533. doi: 10.1073/pnas.2534343100
Marchetti M, Sirard JC, Sansonetti P, Pringault E, Kernéis S. 2004. Interaction of pathogenic bacteria with rabbit appendix M cells: bacterial motility is a key feature in vivo. *Microbes and Infection* **6**:521–528. doi: 10.1016/j.micinf.2004.02.009
McCoy AJ, Grosse-Kunstleve RW, Adams PD, Winn MD, Storoni LC, Read RJ. 2007. Phaser crystallographic software. *Journal of Applied Crystallography* **40**:658–674. doi: 10.1107/S0021889807021206
Mizianty MJ, Stach W, Chen K, Kedarisetti KD, Disfani FM, Kurgan L. 2010. Improved sequence-based prediction of disordered regions with multilayer fusion of multiple information sources. *Bioinformatics* **26**:i489–496. doi: 10.1093/bioinformatics/btq373
Nielsen SS, Toft KN, Snakenborg D, Jeppesen MG, Jacobsen JK, Vestergaard B, Kutter JP, Arleth L. 2009. BioXTAS RAW , a software program for high-throughput automated small-angle X-ray scattering data reduction and preliminary analysis. *Journal of Applied Crystallography* **42**:959–964. doi: 10.1107/S0021889809023863
Philo JS. 2006. Improved methods for fitting sedimentation coefficient distributions derived by time-derivative techniques. *Analytical Biochemistry* **354**:238–246. doi: 10.1016/j.ab.2006.04.053
Prilusky J, Felder CE, Zeev-Ben-Mordehai T, Rydberg EH, Man O, Beckmann JS, Silman I, Sussman JL. 2005. FoldIndex: a simple tool to predict whether a given protein sequence is intrinsically unfolded. *Bioinformatics* **21**:3435–3438. doi: 10.1093/bioinformatics/bti537
Romero P, Obradovic Z, Li X, Garner EC, Brown CJ, Dunker AK. 2001. Sequence complexity of disordered protein. *Proteins* **42**:38–48. doi: 10.1002/1097-0134(20010101)42:1<38::AID-PROT50>3.0.CO;2-3
Schneider TR, Sheldrick GM. 2002. Substructure solution with SHELXD. *Acta Crystallographica Section D Biological Crystallography* **58**:1772–1779. doi: 10.1107/S0907444902011678
Schneidman-Duhovny D, Hammel M, Sali A. 2010. FoXS: a web server for rapid computation and fitting of SAXS profiles. *Nucleic Acids Research* **38**:W540–544. doi: 10.1093/nar/gkq461
Shibata S, Alam M, Aizawa S. 2005. Flagellar filaments of the deep-sea bacteria Idiomarina loihiensis belong to a family different from those of Salmonella typhimurium. *Journal of Molecular Biology* **352**:510–516. doi: 10.1016/j.jmb.2005.07.023

Stafford WF. 1992. Boundary analysis in sedimentation transport experiments: a procedure for obtaining sedimentation coefficient distributions using the time derivative of the concentration profile. *Analytical Biochemistry* **203**:295–301. doi: 10.1016/0003-2697(92)90316-Y

Stafford WF. 1997. Sedimentation velocity spins a new weave for an old fabric. *Current Opinion in Biotechnology* **8**:14–24. doi: 10.1016/S0958-1669(97)80152-8

Svergun DI, Koch MHJ. 2003. Small-angle scattering studies of biological macromolecules in solution. *Reports on Progress in Physics* **66**:1735–1782. doi: 10.1088/0034-4885/66/10/R05

Svergun DI, Petoukhov MV, Koch MH. 2001. Determination of domain structure of proteins from X-ray solution scattering. *Biophysical Journal* **80**:2946–2953. doi: 10.1016/S0006-3495(01)76260-1

Svergun DI. 1992. Determination of the regularization parameter in indirect-transform methods using perceptual criteria. *Journal of Applied Crystallography* **25**:495–503. doi: 10.1107/S0021889892001663

Tang G, Peng L, Baldwin PR, Mann DS, Jiang W, Rees I, Ludtke SJ. 2007. EMAN2: an extensible image processing suite for electron microscopy. *Journal of Structural Biology* **157**:38–46. doi: 10.1016/j.jsb.2006.05.009

Terwilliger TC, Berendzen J. 1999. Automated MAD and MIR structure solution. *Acta Crystallographica Section D Biological Crystallography* **55**:849–861. doi: 10.1107/S0907444999000839

Terwilliger TC. 2000. Maximum-likelihood density modification. *Acta Crystallographica Section D Biological Crystallography* **56**:965–972. doi: 10.1107/S0907444900005072

Van Duyne GD, Standaert RF, Karplus PA, Schreiber SL, Clardy J. 1993. Atomic structures of the human immunophilin FKBP-12 complexes with FK506 and rapamycin. *Journal of Molecular Biology* **229**:105–124. doi: 10.1006/jmbi.1993.1012

Vonderviszt F, Imada K, Furukawa Y, Uedaira H, Taniguchi H, Namba K. 1998. Mechanism of self-association and filament capping by flagellar HAP2. *Journal of Molecular Biology* **284**:1399–1416. doi: 10.1006/jmbi.1998.2274

Wang L, Sauer UH. 2008. OnD-CRF: predicting order and disorder in proteins using [corrected] conditional random fields. *Bioinformatics* **24**:1401–1402. doi: 10.1093/bioinformatics/btn132

Weis DD, Wales TE, Engen JR, Hotchko M, Ten Eyck LF. 2006. Identification and characterization of EX1 kinetics in H/D exchange mass spectrometry by peak width analysis. *Journal of the American Society for Mass Spectrometry* **17**:1498–1509. doi: 10.1016/j.jasms.2006.05.014

Winn MD, Ballard CC, Cowtan KD, Dodson EJ, Emsley P, Evans PR, Keegan RM, Krissinel EB, Leslie AG, McCoy A, McNicholas SJ, Murshudov GN, Pannu NS, Potterton EA, Powell HR, Read RJ, Vagin A, Wilson KS. 2011. Overview of the CCP4 suite and current developments. *Acta Crystallographica Section D Biological Crystallography* **67**:235–242. doi: 10.1107/S0907444910045749

Yang ZR, Thomson R, McNeil P, Esnouf RM. 2005. RONN: the bio-basis function neural network technique applied to the detection of natively disordered regions in proteins. *Bioinformatics* **21**:3369–3376. doi: 10.1093/bioinformatics/bti534

Yonekura K, Maki S, Morgan DG, DeRosier DJ, Vonderviszt F, Imada K, Namba K. 2000. The bacterial flagellar cap as the rotary promoter of flagellin self-assembly. *Science* **290**:2148–2152. doi: 10.1126/science.290.5499.2148

Yonekura K, Maki-Yonekura S, Namba K. 2003. Complete atomic model of the bacterial flagellar filament by electron cryomicroscopy. *Nature* **424**:643–650. doi: 10.1038/nature01830

Zhang T, Faraggi E, Xue B, Dunker AK, Uversky VN, Zhou Y. 2012. SPINE-D: accurate prediction of short and long disordered regions by a single neural-network based method. *Journal of Biomolecular Structure and Dynamics* **29**:799–813. doi: 10.1080/073911012010525022